A Methodology to Determine Work Material Flow Stress and Tool-Chip Interfacial Friction Properties by Using Analysis of Machining

Tuğrul Özel[1]
e-mail: ozel@rci.rutgers.edu

Erol Zeren

Department of Industrial and Systems Engineering,
Rutgers University,
Piscataway, NJ 08854

In this paper, we develop a methodology to determine flow stress at the machining regimes and friction characteristics at the tool-chip interface from the results of orthogonal cutting tests. We utilize metal cutting analysis originally developed by late Oxley and present some improvements. We also evaluate several temperature models in calculating the average temperatures at primary and secondary deformation zones and present comparisons with the experimental data obtained for AISI 1045 steel through assessment of machining models (AMM) activity. The proposed methodology utilizes measured forces and chip thickness obtained through a basic orthogonal cutting test. We conveniently determine work material flow stress at the primary deformation zone and the interfacial friction characteristics along the tool rake face. Calculated friction characteristics include parameters of the normal and frictional stress distributions on the rake face that are maximum normal stress $\sigma_{N\max}$, power exponent for the normal stress distribution, a, length of the plastic contact, l_p, length of the tool-chip contact, l_c, the average shear flow stress at tool-chip interface, k_{chip}, and an average coefficient of friction, μ_e, in the sliding region of the tool-chip interface. Determined flow stress data from orthogonal cutting tests is combined with the flow stress measured through split-hopkinson pressure bar (SHPB) tests and the Johnson-Cook work material model is obtained. Therefore, with this methodology, we extend the applicability of a Johnson-Cook work material model to machining regimes. [DOI: 10.1115/1.2118767]

1 Introduction

Modeling metal cutting processes with the aid of plasticity theory has been a great interest to researchers. The earliest model to describe the metal cutting process is based on the shear plane assumption of Ernst and Merchant [1]. Improvements to this model have been made by Lee and Schaffer [2] in which rigid-plastic workpiece material is assumed and slip-line field analysis is used to model the shear zone. Later, cutting models that included friction, and material behavior at high strains, strain rates, and temperatures are followed [3–5]. The most significant contribution to the field is the parallel-sided shear zone theory introduced by Oxley and co-workers [6]. They developed a model for orthogonal cutting to predict forces and average temperatures and stresses in the deformation zones by using (1) flow stress data of the work material as a function of strain and velocity-modified temperature which couples strain rate to temperature, (2) thermal properties of the work material, (3) tool geometry, and (4) cutting conditions.

In metal cutting, work material goes severe deformations and shearing, specifically, at very high deformation rates and temperatures. Work material flow stress determined through tensile and/or compression tests may not be valid to represent deformation behavior in the ranges of strain, strain rate, and temperature observed during, especially, high-speed machining. In addition, friction between work material and cutting tool surface plays a significant role upon predicted or simulated force, stress and temperature distributions. It has been widely reported that a good understanding of metal cutting mechanics and reliable work material flow stress data and friction properties between the work material and the cutting tool edges must be generated for high speed cutting conditions where typically strain rates up to 10^6 s^{-1} and temperatures up to 1200°C are possible [7–11].

On the other hand, there has been a considerable amount of research devoted to developing the finite element method (FEM) based on numerical models in order to simulate metal cutting processes. FEM based models are highly essential in predicting chip formation, computing forces, distributions of strain, strain rate, temperature, and stress in cutting zones; the chip and the machined work surface as long as accurate work material flow stress models in the function of strain, strain rate, and temperatures are available, and friction characteristics between the cutting tool and the workpiece interfaces are known [7,8,12].

2 Johnson-Cook Material Model

The flow stress models that describe the work material behavior as a function of temperature, strain and strain rate, are considered highly necessary to represent work material constitutive behavior under high-speed cutting conditions for work materials. Unfortunately sound theoretical models based on atomic level material behavior are far from being materialized as reported by Jaspers and Dautzenberg [9]. Therefore, semiempirical constitutive models are widely utilized. Among such models, the constitutive model proposed by Johnson and Cook [13] describes the flow stress of a material with the product of strain, strain rate, and temperature effects that are individually determined as given in Eq. (1),

[1]Author to whom correspondence should be addressed.

Contributed by the Manufacturing Engineering Division of ASME for publication in the JOURNAL OF MANUFACTURING SCIENCE AND ENGINEERING. Manuscript received November 30, 2004; final manuscript received June 3, 2005. Review conducted by A. J. Shih.

Table 1 Material constants for the Johnson-Cook model obtained from SHPB tests

Material	Reference	T_m (°C)	A (MPa)	B (MPa)	C	n	m
AISI 1045	[9]	1460	553.1	600.8	0.0134	0.234	1
Al 6082-T6	[9]	582	428.5	327.7	0.00747	1.008	1.31
Ti6Al4V	[17]	1630	862.5	331.2	0.0120	0.34	0.8
Ti6Al4V	[16]	1630	782.7	498.4	0.028	0.28	1.0

$$\bar{\sigma} = [A + B(\bar{\varepsilon})^n]\left[1 + C\ln\left(\frac{\dot{\bar{\varepsilon}}}{\dot{\bar{\varepsilon}}_0}\right)\right]\left[1 - \left(\frac{T - T_0}{T_m - T_0}\right)^m\right] \quad (1)$$

In the Johnson-Cook (JC) constitutive model, the parameter A is the initial yield strength of the material at room temperature and a strain rate of 1 s^{-1} and $\bar{\varepsilon}$ represents the plastic equivalent strain. The equivalent plastic strain rate $\dot{\bar{\varepsilon}}$ is normalized with a reference strain rate $\dot{\bar{\varepsilon}}_0$. The temperature term in the JC model reduces the flow stress to zero at the melting temperature of the work material, T_m, leaving the constitutive model with no temperature effect. In general, the constants A, B, C, n, and m of the model are fitted to the data obtained by several material tests conducted at low strains and strain rates and at room temperature as well as the split Hopkinson pressure bar (SHPB) tests at strain rates up to 10^4 s^{-1} and at temperatures up to 600°C [8,9]. The JC model provides a good fit for strain-hardening behavior of metals and it is numerically robust and can easily be used in FEM simulation models [9]. Zerilli and Armstrong (ZA) derived an alternative constitutive model for metals with a crystal structure distinction by using dislocation-mechanics theory [14].

Many researchers used the JC constitutive model for deformation behavior of metal alloys at high strain rate and temperatures and identified the material constants from SHPB tests [9,13,15–17]. Among those, Lee and Lin [16] presented a JC model for high temperature deformation behavior of a titanium alloy, Ti6Al4V, obtained from SHPB test results at a strain rate of 2000 s^{-1} but temperatures up to 1100°C. Meyer and Kleponis [17] also studied high strain rate behavior of Ti6Al4V and fitted their experiments into the JC constitutive model obtained at strain rates up to 2150 s^{-1} and at room temperatures. Both research groups also discussed advantages and disadvantages of using the JC constitutive model for Ti6A4V. Jaspers and Dautzenberg [9] developed both JC and ZA models for AISI 1045 steel and Al 6082-T6 aluminum to account for deformations at high strain rates and temperatures by utilizing SHPB test results. All of those studies indicate that SHPB tests are capable of generating flow stress data at high strain rate and temperature but not at the levels observed in cutting regimes. In this paper, we are only concerned with three materials selected to benchmark the methodology presented and there are AISI 1045 steel, Al 6082-T6 aluminum, and Ti6Al4V titanium alloys (see Table 1).

3 Determination of Work Flow Stress From Orthogonal Cutting Tests

In the past, some researchers utilized the orthogonal cutting process as a material property test in order to obtain work material flow stress data. Among them, Shatla et al. [18] used Oxley's parallel sided thin shear zone orthogonal cutting model and empirically determined constants of the modified JC model by applying orthogonal high-speed slot milling experimentation technique [12]. They presented some findings for the modified JC model for tool steels AISI P20 and AISI H13, and aluminum, Al 2007. Tounsi et al. [19] formulated an analytical model for orthogonal cutting to identify variables of the JC constitutive model. They applied the least-square estimator method to obtain variables of the JC constitutive model. Thickness of the primary shear zone is assumed constant and it is approximated as one-half of the uncut chip thickness. They presented JC models for 42CD4U steel, S300 steel, 316L stainless steel, and 35NCD16 steel. Adibi et al. [10,20] extended Oxley's analysis and applied to different material models including the JC constitutive model.

Experimental evidence presented by Zorev [3], Childs [8], and Lee et al. [21] depicted that the normal and frictional stress distributions are not uniform over the tool rake face. However, Oxley's model assumes that the normal and frictional stress is constant at the tool rake face [6]. The studies reviewed in determining flow stress and using the JC work material model [10,18–20] used Oxley's assumption and have presented no new solutions to interfacial friction that take place at the tool-chip interface.

In this paper, we aim to determine the constants of the JC constitutive model as work material flow stress at excessive strain, strain rate and temperature regimes as well as interfacial friction at tool-chip interface by utilizing orthogonal cutting test results that include measured values of machining forces and chip thickness. The constants of the JC model are computed by applying Oxley's slip-line field analysis in reverse [6]. An experimentally determined slip-line field analysis, which is originally proposed by Tay et al. [4], is used for the secondary deformation zone. The orthogonal cutting test results are used in determining stress distributions on tool rake face and hence the frictional constants at tool-chip interface. The analysis presented in this paper is based on continuous chip formation assumption.

4 Oxley's Analysis of Machining

A simplified illustration of the plastic deformation for the formation of a continuous chip when machining a ductile material is given in Fig. 1. There are two deformation zones in this simplified model—a primary zone and a secondary zone. It is commonly recognized that the primary plastic deformation takes place in a finite-sized shear zone. The work material begins to deform when it enters the primary zone from lower boundary *CD*, and it continues to deform as the material streamlines follow smooth curves

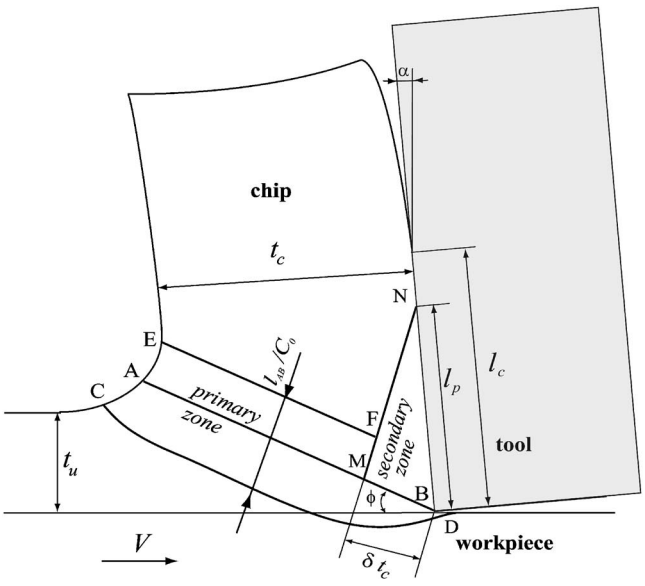

Fig. 1 Simplified deformation zones in orthogonal cutting

until it passes the upper boundary *EF*. Oxley and co-workers [6] assumed that the primary zone is a parallel-sided shear zone. There is also a secondary deformation zone adjacent to the tool-chip interface that is caused by the intense contact pressure and frictional force. After exiting from the primary deformation zone, some material experiences further plastic deformation in the secondary deformation zone. Using the quick-stop method to experimentally measure the flow field, Oxley [6] proposed a slip-line field similar to the one shown in Fig. 1. Initially, Oxley and co-workers assumed that the secondary zone is a constant thickness shear zone. In this study, we assume that the secondary deformation zone is triangular shape and the maximum thickness is proportional to the chip thickness, i.e., δt_c.

The slip-line field and the corresponding hodograph indicated that the strain rate in the primary deformation zone increases with cutting speed and has a maximum value at plane *AB*. Based on this experimental observations, Oxley proposed the empirical relation in Eq. (2) for the average value of the shear strain rate along *AB*,

$$\dot{\gamma}_{AB} = C_0 \frac{V_S}{l_{AB}} \tag{2}$$

The velocity along the shear plane is

$$V_S = \frac{V \cos \alpha}{\cos(\phi - \alpha)} \tag{3}$$

In Eq. (2), C_0 is a material and cutting condition dependent constant representing the ratio of the thickness of the primary zone to the length of plane *AB*. The shear angle can be estimated from Eq. (4),

$$\phi = \tan^{-1}\left(\frac{\frac{t_u}{t_c}\cos \alpha}{1 - \frac{t_u}{t_c}\sin \alpha} \right) \tag{4}$$

Oxley and co-workers [6] found that material constant C_0 is cutting condition dependent but approximated that $C_0 = 5.9$ for the mild steel used in their experiments. Although the strain rate is slightly higher in the vicinity of the tool cutting edge, its value remains relatively constant over the majority of plane *AB* [6]. The shear strain occurring in the primary deformation zone, and therefore corresponds to the average shear strain in the primary deformation zone,

$$\gamma_{AB} = \frac{\cos \alpha}{2 \sin \phi \cos(\phi - \alpha)} \tag{5}$$

In the primary zone, the shear stress stays the same on plane *AB*, and the average value of shear stress at *AB* is given by Eq. (6),

$$k_{AB} = \frac{F_S \sin \phi}{t_u w} \tag{6}$$

The shear force F_S is calculated from the measured cutting force F_C and feed force F_T, as shown in Eq. (7),

$$F_S = F_C \cos \phi - F_T \sin \phi \tag{7}$$

Huang and Liang [22] used Oxley's model and applied it to force prediction in CBN hard turning. Adibi et al. [10,20] extended Oxley's analysis of orthogonal cutting to use for carbon steels AISI 1020 and AISI 1040 steels, as well as aluminum alloys Al 2024-T3, Al 6061-T6, and Al 6082-T6.

4.1 Assessment of Temperature Models. Due to the difficulties associated with routinely measuring meaningful machining temperatures, developing mathematical models for machining temperature has been widely used as an attractive alternative. Earlier analytical work on the steady-state temperatures generated during metal cutting was due to Trigger and Chao [23], Chao and Trigger [24], Loewen and Shaw [25], and Leone [26]. Many other analytical models are introduced later including the model of Boothroyd [27] as modified by Oxley and co-workers [6]. Recently, two new temperature models are introduced by Tounsi et al. [19] and Adibi et al. [10]. All of these temperature models consider an average temperature rise due to shearing in the primary deformation zone and a temperature rise due to additional shearing and friction in the secondary deformation zone. Komanduri and Hou [28] proposed a more detailed thermal modeling approach based on oblique moving heat source theory to predict temperature fields instead of average temperatures in orthogonal cutting. We only consider temperature models for predicting average temperatures in the primary and secondary deformation zones, for simplicity in implementing into proposed methodology to determine flow stress and friction parameters (Fig. 2).

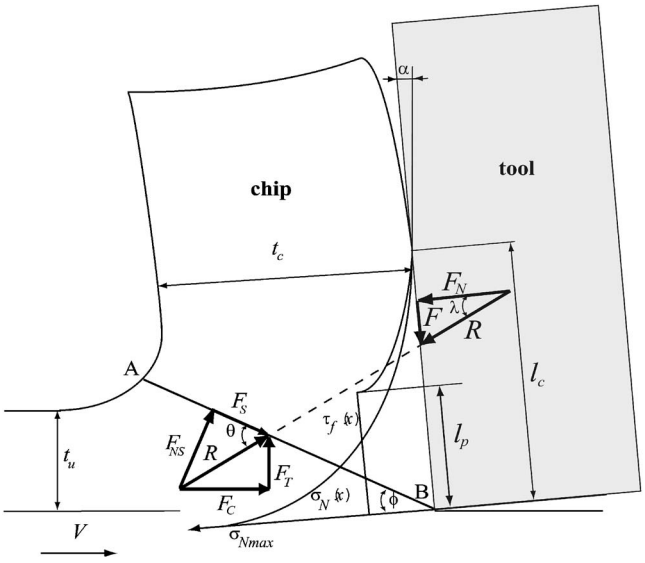

Fig. 2 Forces acting on the shear plane and the tool with resultant stress distributions on the tool rake face

Oxley and co-workers [6] utilized a modified Boothroyd's temperature model [27] and used it in their analysis. In this model, the temperature rise at the primary shear zone is given by Eq. (8),

$$T_{AB} = T_0 + \Delta T_{AB} \tag{8a}$$

$$\Delta T_{AB} = \frac{(1 - \beta) F_S \cos \alpha}{\rho S t_u w \cos(\phi - \alpha)} \tag{8b}$$

where

$$\beta = 0.5 - 0.35 \log(R_T \tan \phi) \text{ for } 0.04 \leq R_T \tan \phi \leq 10.0 \tag{9a}$$

$$\beta = 0.3 - 0.15 \log(R_T \tan \phi) \text{ for } R_T \tan \phi > 10.0 \tag{9b}$$

$$R_T = \frac{\rho S V t_u}{K} \tag{10}$$

The average tool-chip interface temperature is the average temperature at the primary zone plus the maximum temperature in the chip that is given in Eq. (11),

$$T_{\text{int}} = T_{AB} + \psi \Delta T_M \tag{11}$$

The maximum temperature rise in the chip, ΔT_M and the interface temperature factor ψ can be calculated, once the thickness of the tool-chip interface δt_c, and tool-chip contact length l_c are found,

Table 2 Conditions of orthogonal cutting tests performed for AISI 1045 carbon steel in AMM activity [29]

Test	V (m/min)	t_u (mm)	t_c (mm)	α (deg)
1	200	0.150	0.518	−7
2	200	0.150	0.476	+5
3	200	0.300	0.892	−7
4	200	0.300	0.691	+5
5	300	0.150	0.671	−7
6	300	0.150	0.412	+5
7	300	0.300	0.715	−7
8	300	0.300	0.772	+5

$$\log\left(\frac{\Delta T_M}{\Delta T_C}\right) = 0.06 - 0.195\delta\left(\frac{R_T t_c}{l_c}\right)^{1/2} + 0.5\log\left(\frac{R_T t_c}{l_c}\right) \tag{12a}$$

The average temperature rise in chip, ΔT_C, is given by

$$\Delta T_C = \frac{F_F \sin\phi}{\rho S t_u w \cos(\phi - \alpha)} \tag{12b}$$

The tool-chip contact length, l_c, can be found by

$$l_c = \frac{t_u \sin\theta}{\cos\lambda \sin\phi}\left(1 + \frac{C_0 n}{3\left[1 + 2\left(\frac{\pi}{4} - \phi\right) - C_0 n\right]}\right) \tag{13}$$

where the angles θ and λ are given with Eqs. (14) and (15).

$$\tan\theta = 1 + 2\left(\frac{\pi}{4} - \phi\right) - C_0 n \tag{14}$$

$$\lambda = \theta - \phi + \alpha \tag{15}$$

In this study, we present an assessment of temperature models proposed by various machining researchers in order to identify a model that is in closest agreement with experiments. For this purpose, the cutting test data obtained for AISI 1045 steel during the assessment of machining models (AMM) activity [29], which is summarized in Table 2, has been utilized. The comparison of the predicted forces and average temperatures along AB and at the tool-chip interface with experiments is shown in Figs. 3–6, respectively. It is convincing that good agreements between the predicted and measured forces and temperatures are obtained when using a temperature model proposed by Oxley and co-workers [6].

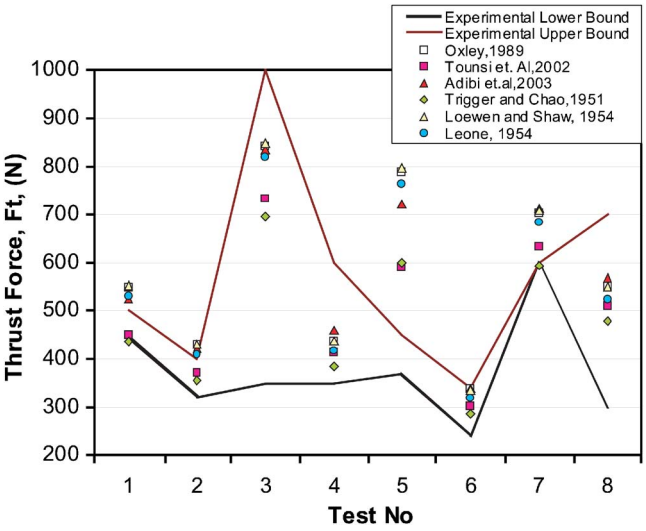

Fig. 4 Comparison of predicted thrust forces with experiments [29] for various temperature models in machining AISI 1045 steel

4.2 Determination of Strain, Strain Rate, Temperature, and Flow Stress in the Primary Deformation Zone. The average shear strain rate, shear strain, and shear stress in the primary deformation zone are given by Eqs. (2), (5), and (6), respectively. Using the Von Mises criterion, they can be related to the equivalent stress, strain, and strain rate using Eq. (16),

$$\bar{\sigma}_{AB} = \sqrt{3}k_{AB}, \quad \bar{\varepsilon}_{AB} = \frac{\gamma_{AB}}{\sqrt{3}}, \quad \dot{\bar{\varepsilon}}_{AB} = \frac{\dot{\gamma}_{AB}}{\sqrt{3}} \tag{16}$$

In order to determine the constants of the JC constitutive model, a set of orthogonal cutting experiments is performed to measure the forces F_C and F_T in various cutting conditions and later values of $\bar{\varepsilon}_{AB}$, $\dot{\bar{\varepsilon}}_{AB}$, $\bar{\sigma}_{AB}$, and T_{AB} are computed.

Identifying the best fit for the constants of JC model, A, B, C, m, n is in fact quite challenging due to the high nonlinearity imposed when using inverse solution of Oxley's analysis

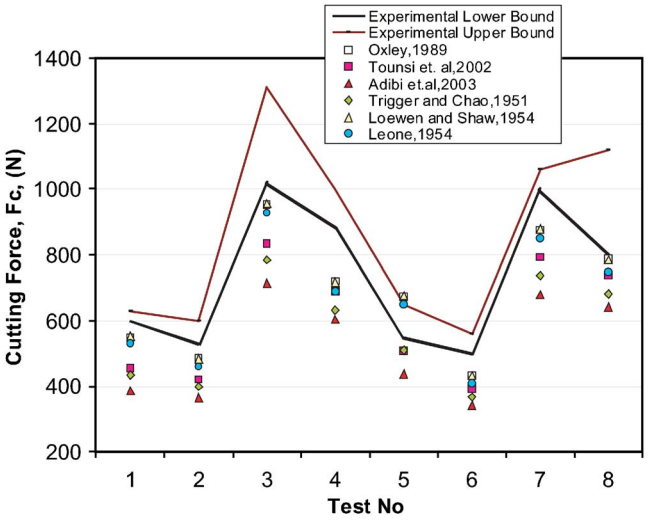

Fig. 3 Comparison of predicted cutting forces with experiments [29] for various temperature models in machining AISI 1045 steel

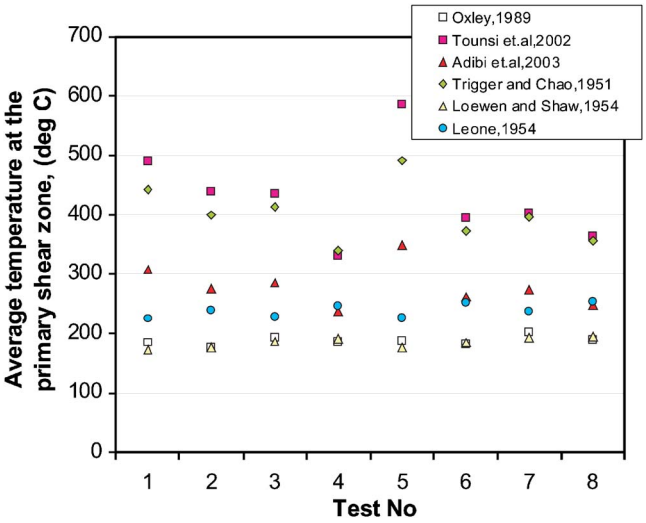

Fig. 5 Comparison of predicted average temperature at the primary zone for various temperature models in machining AISI 1045 steel

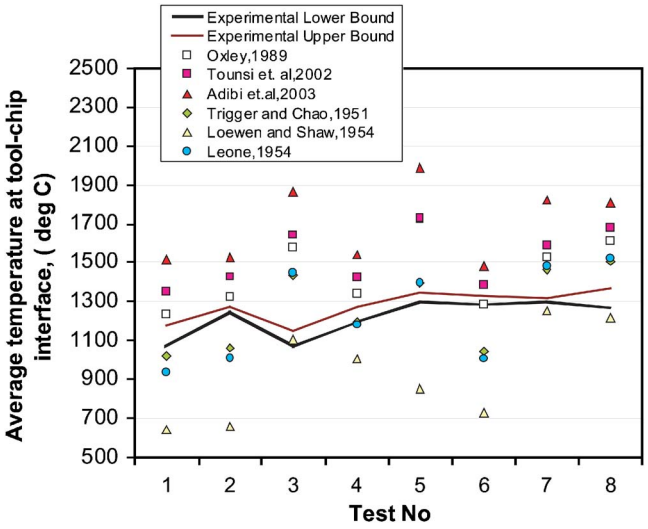

Fig. 6 Comparison of predicted average temperature at tool-chip interface with experiments [29] for various temperature models in machining AISI 1045 steel

of machining. Other researchers proposed various techniques to address this problem. For instance, Shatla et al. [18] reported that their algorithm is vulnerable finding local convergence as the unrealistic combinations of JC constants as the solution.

In this study, the constants of JC model are determined by using a nonlinear regression solution based on the Gauss-Newton algorithm with Levenberg-Marquardt modifications for better global convergence [30]. The only unknown value at this point is C_0, which is given by Eq. (17),

$$C_0 = \frac{(p_A - p_B)(A\bar{\varepsilon}_{AB}^{-n} + B)}{2Bnk_{AB}} \tag{17a}$$

$$p_A = k_{AB}\left[1 + 2\left(\frac{\pi}{4} - \phi\right)\right] \tag{17b}$$

$$p_B = \frac{2F_{NS}\sin\phi}{t_u w} - p_A \tag{17c}$$

In Eq. (17*a*), p_A and p_B are the hydrostatic stresses at points A and B, respectively, which can be determined from measured machining forces and stress state at point A as shown in Eqs. (17*b*) and (17*c*) [6]. The parameter C_0 is solved in an iterative procedure and the constants of the JC constitutive model are computed (Fig. 7). Therefore, the determined JC constitutive model as work material flow stress can be directly used in the FEM simulations of metal cutting.

5 Analytical Model for Tool-Chip Interfacial Friction

Interfacial friction on the tool rake face is not continuous and is a function of the normal and frictional stress distributions. According to Zorev [3], the normal stress is greatest at the tool tip and gradually decreases to zero at the point where the chip separates from the rake face as shown in Fig. 2. The frictional shearing stress distribution is more complicated. Over the portion of the tool-chip contact area near the cutting edge, sticking friction occurs, and the frictional shearing stress, τ_{int} is equal to average shear flow stress at tool-chip interface in the chip, k_{chip}. Over the remainder of the tool-chip contact area, sliding friction occurs, and the frictional shearing stress can be calculated using the coefficient of friction μ_e. This section describes a methodology to determine the shearing stress in the sticking region and the coefficient of friction in the sliding region, based on the measured machining forces, F_C and F_T, and the measured (or calculated) tool-chip interface contact length l_c.

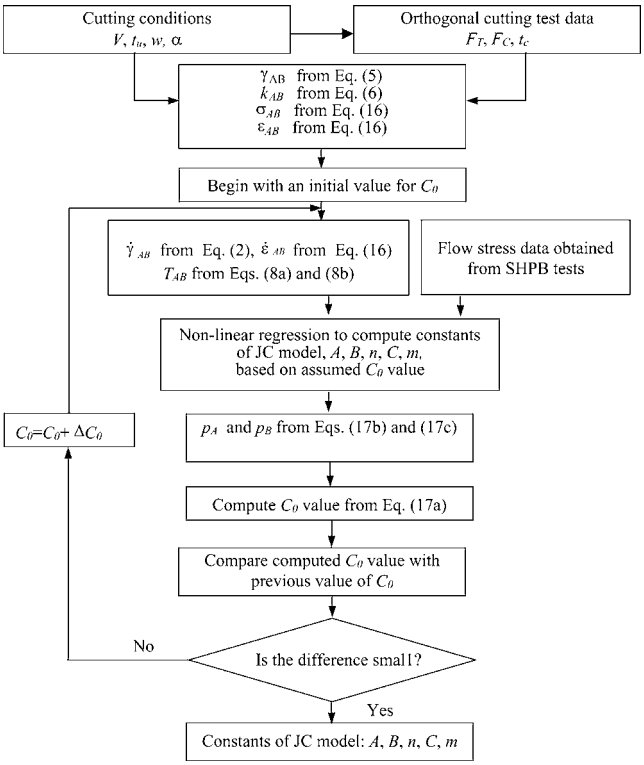

Fig. 7 Flow chart for the methodology to determine work material flow stress

The normal stress distribution on the tool rake face can be described by Eq. (18)

$$\sigma_N(x) = \sigma_{N_{\max}}\left[1 - \left(\frac{x}{l_c}\right)^a\right] \tag{18}$$

In Eq. (18), x is the distance from the cutting edge, and a is the power exponent that must be calculated. Integrating the normal stress along the entire tool-chip contact length yields the relation in Eq. (19),

$$F_N = \int_0^{l_c} w\sigma_N(x)dx = \int_0^{l_c} w\sigma_{N_{\max}}\left[1 - \left(\frac{x}{l_c}\right)^a\right]dx \tag{19}$$

F_N is the normal force on the tool rake face determined from Eq. (20)

$$F_N = F_C\cos\alpha - F_T\sin\alpha \tag{20}$$

Oxley [6] showed that $\sigma_{N_{\max}}$ can be estimated by analyzing the hydrostatic stress along AB, yielding Eq. (21),

$$\sigma_{N_{\max}} = k_{AB}\left(1 + \frac{\pi}{2} - 2\alpha - 2\frac{BnC_0}{A\bar{\varepsilon}_{AB}^{-n} + B}\right) \tag{21}$$

Combining Eqs. (19)–(21), it can be shown that the power exponent a is obtained as given in Eq. (22),

$$a = \frac{F_N}{wl_C k_{AB}\left(1 + \frac{\pi}{2} - 2\alpha - 2\frac{BnC_0}{A\bar{\varepsilon}_{AB}^{-n} + B}\right) - F_N} \tag{22}$$

Normal stress distribution over the rake face is fully defined and the coefficient of friction can be computed, once the values of the parameters $\sigma_{N_{\max}}$ and a are found. The shear stress distribution on the tool rake face illustrated in Fig. 2 can be represented in two

distinct regions: (a) in the sticking region: $\tau_{\text{int}}(x)=k_{\text{chip}}$ and when $\mu_e\sigma_N(x)\geq k_{\text{chip}}$, $0<x\leq l_P$; (b) in the sliding region: $\tau_{\text{int}}(x)=\mu_e\sigma_N(x)$ and when $\mu_e\sigma_N(x)<k_{\text{chip}}$, $l_P<x\leq l_C$. Here k_{chip} is the shear flow stress of the material at tool-chip interface in the chip and it is related to the frictional force between the chip and the tool, F_F, which is given in Eq. (23),

$$F_F=\int_0^{l_P} wk_{\text{chip}}dx+\int_{l_P}^{l_C} w\mu_e\sigma_N(x)dx \tag{23}$$

The relation between the average coefficient of friction in the sliding region μ_e and k_{chip} is also given in Eq. (24).

$$\mu_e=\frac{k_{\text{chip}}}{\sigma_N(l_P)} \tag{24}$$

Combining Eqs. (23) and (24) leads to the expression for k_{chip} as shown in Eq. (25)

$$k_{\text{chip}}=\frac{F_F}{wl_P+\dfrac{w}{\sigma_N(l_P)}\displaystyle\int_{l_p}^{l_C}\sigma_N(x)dx} \tag{25}$$

The frictional force component F_F is given by Eq. (26).

$$F_F=F_C\sin\alpha+F_T\cos\alpha \tag{26}$$

As shown in Fig. 1, the shape of the secondary plastic zone in the sticking region can be assumed triangular according to Tay et al. [4]. On the rake face point N is located at the interface between the sticking and sliding regions. Line MN is a type II slip-line that is assumed to be straight. A similar approach proposed by Oxley [6] can be taken to analyze hydrostatic stresses along MN, and to compute the length of sticking region, l_P using Eq. (27),

$$l_P=\frac{\delta\,.\,t_c}{\sin(\phi-\alpha)} \tag{27}$$

The maximum thickness of the secondary zone is $\delta.t_c$ as shown in Fig. 1 and δ is another parameter yet to be determined iteratively. According to Oxley [6], the average shear strain rate and shear strain are considered constant and can be estimated from Eqs. (28) and (29) in the secondary zone.

$$\dot{\gamma}_{\text{int}}=\frac{V_C}{\delta t_c} \tag{28}$$

$$\gamma_{\text{int}}=\frac{l_P}{\delta t_c} \tag{29}$$

The shear flow stress, shear strain rate, shear strain, and temperature for the secondary zone are given by Eqs. (25), (28), (29), and (13), respectively. The only unknown in the solution process is the value of δ which is often solved based on the minimum work criterion proposed by Oxley [6]. As derived in the Appendix, the difference between hydrostatic stresses at points M and N (p_M and p_N, respectively) is given again in Eq. (30*a*),

$$p_M-p_N=k_{\text{chip}}\left[2(\phi-\alpha)+\left(\frac{(Bn\bar{\varepsilon}_{\text{int}}^{n})/\gamma_{\text{int}}}{A+B\bar{\varepsilon}_{\text{int}}^{n}}\right)\frac{l_p\sin\phi}{\delta t_c\sin(\phi-\alpha)}\right] \tag{30a}$$

As shown in Fig. 1, point M is on line AB, and p changes proportionally along AB as $p_B<p_A$ remains and the hydrostatic stress at point M can be given as Eq. (30*b*),

$$p_M=p_B+\frac{\delta t_c}{l_{AB}}(p_A-p_B) \tag{30b}$$

The hydrostatic stress at point N is equal to the normal stress at l_p as shown in Eq. (31),

$$p_N=\sigma_N(l_p) \tag{31}$$

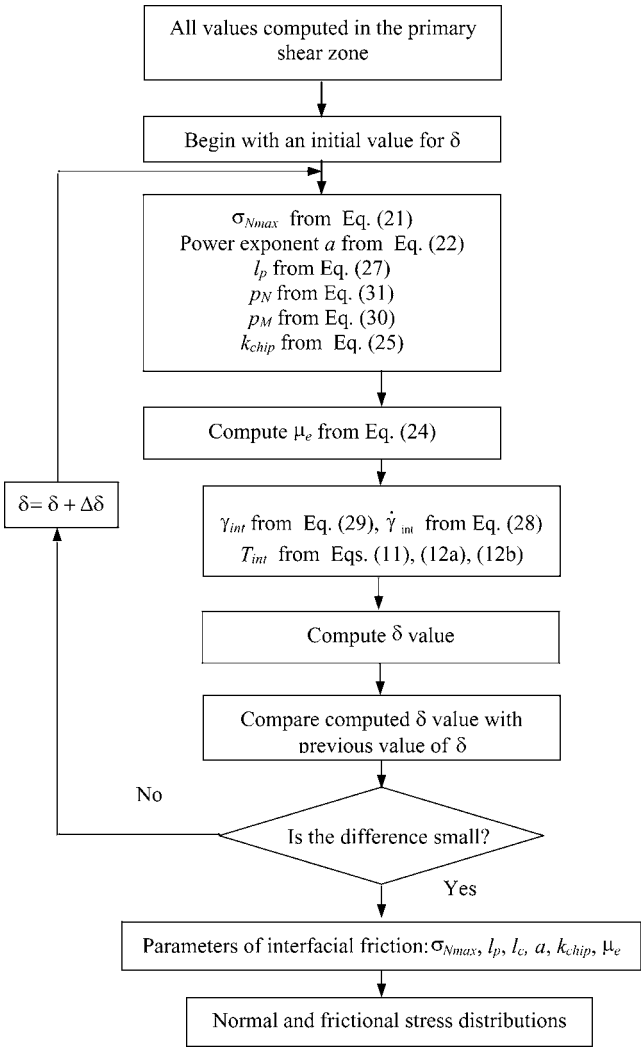

Fig. 8 Flow chart for the methodology to determine the parameters of tool-chip interfacial friction as normal and frictional stress distributions

The only unknown in Eqs. (29), (30), and (31), δ, is solved in an iterative procedure and together with the frictional parameters; k_{chip}, τ_{int}, $\sigma_{N_{\max}}$, l_p, l_c, a, and μ_e, is determined as part of the entire determination of the work material flow stress and frictional parameters at the tool-chip interface using orthogonal cutting tests (Fig. 8).

6 Results

The goal of this work is to present a methodology in order to determine work material flow stress as the deformation rates arise in machining and estimate friction characteristic at tool-chip interface for use in FEM simulations of metal cutting. For this purpose, a work material constitutive model developed by Johnson and Cook [13] is used as the work material flow stress model. The friction model at the tool-chip interface is based on estimation of normal and frictional stress distributions along the tool rake face. The constants of the JC constitutive model and frictional parameters can be computed in an iteration scheme by utilizing an inverse solution of Oxley's machining theory and orthogonal cutting tests for various cutting conditions. Computed friction parameters include; maximum normal stress on the rake face, $\sigma_{N_{\max}}$, power exponent of the normal stress distribution, a, length of the plastic contact (sticking region) at the tool-chip interface, l_p, tool-chip contact length, l_c, average shear flow stress in the chip, k_{chip}, co-

Table 3 Conditions and measured process variables in orthogonal cutting tests performed for 0.38% carbon steel (w=4 mm, α=−5 deg) [6]

Test	V (m/min)	t_u (mm)	t_c (mm)	ϕ[a] (deg)	F_C (N/mm)	F_T (N/mm)
1	100	0.125	0.4	16.9	350	325
2	200	0.125	0.3	21.8	325	225
3	400	0.125	0.3	21.8	300	225
4	100	0.25	0.7	19.0	625	450
5	200	0.25	0.55	23.5	625	375
6	400	0.25	0.5	25.5	550	325
7	100	0.5	1.1	23.5	1125	625
8	200	0.5	0.9	27.8	1050	500

[a]Calculated by using Eq. (4)

efficient of friction in sliding region of the tool-chip interface, μ_e. The tool-chip interface friction parameters are used in estimation of normal and frictional stress distribution over the rake face.

The methodology presented in this work is used in determining flow stress properties of three benchmark materials, AISI 1045 steel, Al 6082-T6, and Ti6Al4V alloys. The flow stress data obtained from SHPB tests is combined with the flow stress determined under the orthogonal cutting conditions just before running into the nonlinear regression step as shown in the flow chart given in Fig. 8.

6.1 AISI 1045 Steel. The orthogonal cutting tests results for AISI 1045 are adopted from Oxley [6] that are performed for 0.38% carbon steel. The cutting conditions are given in Table 3. The flow stress data of SHPB tests adopted from Jasper and Dautzenberg [18] is combined with the flow stress determined under the orthogonal cutting conditions. The constants of the JC material model for work flow stress are computed as A=451.6, B=819.5, C=0.0000009, n=0.1736, and m=1.0955 for the extended ranges of strain (0.051–1.07), strain-rate ($1-17766\ s^{-1}$) and temperature (20–721°C). Those constants are found in close agreements with the ones determined by Jasper and Dautzenberg [9], as given in Table 1, indicating the success of the proposed methodology. The details of the computed process variables in the primary and secondary deformation zones are given in Table 4. The parameters of the tool-chip interface friction model are also computed by using the methodology proposed in this study as shown in Table 5.

6.2 Al 6082-T6. This methodology is also applied to determine the constants of JC material model for an aluminum alloy, Al 6082-T6. The orthogonal cutting test data is obtained from the work done by Adibi-Sedeh and Mahdavan [10] and given in Table 6. The flow stress data of SHPB tests adopted from Jasper and Dautzenberg [9] is combined with the flow stress determined under the orthogonal cutting conditions. The constants of the JC material model for work material flow stress are computed as A=442.95, B=324.62, C=0.0000010186, n=1.0261, and m=1.3116 for the extended ranges of strain (0.05–0.7889), strain-rate ($1-18295\ s^{-1}$) and temperature (20–510°C). Determined constants of the JC material model are found in close agreement with the ones obtained through SHPB tests by Jasper and Dautzenberg [9] as shown in Table 1. The details of the computed process variables in the primary and secondary deformation zones are given in Table 7. Computed parameters of the tool-chip interface friction model are given in Table 8.

6.3 Ti6Al4V. The same methodology is also applied to determine the constants of the JC material model for Ti6Al4V, a popular aerospace alloy. The orthogonal cutting test data that is utilized in determining flow stress for the titanium alloy Ti6Al4V is taken from the work done by Barry et al. [31] and given in Table 9. Barry et al. stated that the chip formation was continuous with sawtooth shapes and at high cutting speeds a thermoplastic instability occurred. Therefore, we utilized the cutting test data only up to 60 m/min of cutting speed. In each of the cutting conditions given in Table 9, cutting and thrust forces and chip thickness are

Table 4 Computed process variables in the deformation zones and at tool-chip interface in machining 0.38% carbon steel (w=4 mm, α=−5 deg)

Test	$\bar{\varepsilon}_{AB}$	$\dot{\bar{\varepsilon}}_{AB}$	T_{AB}	k_{AB} (N/mm^2)	$\bar{\varepsilon}_{\text{int}}$	$\dot{\bar{\varepsilon}}_{\text{int}}$	T_{int}	k_{chip} (N/mm^2)
1	1.07	5488	428	558.5	1.55	1.50	627	223.8
2	0.87	16488	474	648.6	1.28	5.35	681	188.6
3	0.87	17766	447	579.5	1.28	10.69	701	214.9
4	0.97	5861	467	579.3	1.42	0.98	662	193.6
5	0.82	10632	494	676.1	1.21	3.18	721	206.6
6	0.78	12653	450	614.0	1.14	7.70	674	211.9
7	0.82	3399	458	624.4	1.21	0.79	649	192.9
8	0.73	4814	453	649.0	1.07	2.37	635	191.3

Table 5 Computed parameters of C_0, δ, and tool-chip interfacial friction in machining 0.38% carbon steel (w=4 mm, α=−5 deg)

Test	C_0	δ	$\sigma_{N\,\max}$ (N/mm^2)	l_p (mm)	l_c (mm)	a	k_{chip} (N/mm^2)	μ_e
1	2.39	0.008	1234	0.54	2.5	0.1393	223.8	0.94
2	2.67	0.006	1396	0.33	2.25	0.1228	188.6	0.65
3	1.48	0.008	1401	0.33	1.875	0.1380	214.9	0.72
4	4.38	0.019	1024	0.86	3.75	0.2083	193.6	0.71
5	3.14	0.018	1386	0.58	3.05	0.1834	206.6	0.57
6	1.75	0.020	1450	0.49	2.55	0.1847	211.9	0.56
7	3.99	0.050	1163	1.15	4.95	0.2566	192.9	0.53
8	2.35	0.054	1447	0.83	4.05	0.2284	191.3	0.44

Table 6 Conditions and measured process variables in orthogonal cutting tests performed for Al 6082-T6 (w=3 mm, α=8 deg) [10]

Test	V (m/min)	t_u (mm)	t_c (mm)	ϕ[a] (deg)	F_C (N/mm)	F_T (N/mm)
1	120	0.2	0.52	21.92	180	130
2	240	0.2	0.415	27.09	155	85
3	360	0.2	0.39	28.67	150	70
4	480	0.2	0.375	29.70	140	60
5	120	0.4	0.8	28.02	300	165
6	240	0.4	0.685	32.19	270	105
7	360	0.4	0.605	35.79	255	95
8	480	0.4	0.59	36.55	245	80

[a]Calculated by using Eq. (4)

measured. However, the tool-chip contact conditions are not measured in this experimental work. Therefore, we estimated tool-chip contact length using Eq. (13).

The flow stress data of SHPB tests adopted from Lee and Lin [16] is combined with the flow stress determined under the orthogonal cutting conditions. The determined constants of JC work material constitutive model are given as A=859.55, B=639.75, C=0.000002215, n=0.225, and m=1.112 for the extended ranges of strain (0.05–0.79), strain-rate (1–84993 s^{-1}) and temperature (20–657°C). The comparison of the two sets of JC constants indicate that the developed methodology is practical and it is capable of extending work material flow stress model to the deformation regimes, i.e., high strain rate and high temperature, seen in machining. However it should be noted that the JC material model constant C for strain rate sensitivity has become smaller than the constants obtained from SHPB tests. This is expected, as at the increased cutting speed thermal softening may dominate the strain

Table 7 Computed process variables in the primary and secondary zones in machining of Al 6082-T6 (w=3 mm, α=8 deg)

Test	$\bar{\varepsilon}_{AB}$	$\dot{\bar{\varepsilon}}_{AB}$	T_{AB}	k_{AB} (N/mm^2)	$\bar{\varepsilon}_{\text{int}}$	$\dot{\bar{\varepsilon}}_{\text{int}}$	T_{int}	k_{chip}(N/mm^2)
1	0.7889	3298	175	221	2.3999	1.7081	269	88.2
2	0.6642	8266	184	226	1.7651	5.3637	290	88.2
3	0.6368	13194	199	235	1.6354	9.1101	305	77.9
4	0.6209	18295	194	227	1.5612	13.1379	298	71.2
5	0.6476	2144	177	220	1.6864	1.4434	286	95
6	0.5883	5008	188	229	1.4092	3.9374	294	79.3
7	0.5525	8505	178	221	1.2382	7.5713	294	76.8
8	0.5465	11628	180	222	1.2080	10.6149	292	74.6

Table 8 Computed parameters of C_0, δ, and tool-chip interfacial friction in machining of Al 6082-T6 (w=3 mm, α=8 deg)

Test	C_0	δ	$\sigma_{N\max}$ (N/mm^2)	l_p (mm)	l_c (mm)	a	μ_e
1	0.58814	0.0950	409.2	1.0807	2.5817	0.1786	1.4964
2	0.45541	0.0803	449.3	0.6344	1.9584	0.1919	1.0100
3	0.64571	0.0698	440.5	0.5524	2.0110	0.1858	0.8289
4	0.66492	0.0659	425.3	0.5070	1.9686	0.1843	0.7575
5	0.19139	0.1686	476.5	1.1684	3.4767	0.1983	1.0262
6	0.32318	0.1442	481.2	0.8360	3.1217	0.2023	0.7046
7	0.59483	0.1027	429.9	0.6487	3.2556	0.2062	0.6317
8	0.39266	0.1173	458.3	0.6172	2.8489	0.2155	0.5799

Table 9 Conditions and measured process variables in orthogonal cutting tests performed for Ti6Al4V (w=1.1 mm, α=−6 deg) [31]

Test	V (m/min)	t_u (mm)	t_c (mm)	ϕ[a] (deg)	F_C (N)	F_T (N)
1	15	0.1	0.15	31.79	255	129
2	15	0.08	0.12	31.79	210	114
3	15	0.06	0.0942	30.71	160	84
4	15	0.04	0.0668	29.27	110	54
5	15	0.02	0.041	24.78	45	24
6	30	0.1	0.145	32.61	255.5	123
7	30	0.08	0.116	32.61	215.5	118
8	30	0.06	0.0888	32.11	160.5	88
9	30	0.04	0.064	30.26	110.5	58
10	30	0.02	0.0366	27.21	45.5	18
11	60	0.1	0.132	34.92	241.5	120
12	60	0.08	0.108	34.36	211.5	110
13	60	0.06	0.0852	33.12	156.5	85
14	60	0.04	0.0608	31.48	106.5	60
15	60	0.02	0.0354	27.95	41.5	15

[a]Calculated by using Eq. (4)

Table 10 Computed process variables in the deformation zones and at tool-chip interface in machining Ti6Al4V alloy (w =1.1 mm, α=−6 deg)

Test	$\bar{\varepsilon}_{AB}$	$\dot{\bar{\varepsilon}}_{AB}$	T_{AB}	k_{AB} (N/mm^2)	$\bar{\varepsilon}_{\text{int}}$	$\dot{\bar{\varepsilon}}_{\text{int}}$	T_{int}	k_{chip} (N/mm^2)
1	0.68959	1780	571.03	712.57	0.94217	1.283	806.36	246.5
2	0.68959	3708.3	543.65	709.04	0.94217	1.6038	774.68	249.94
3	0.70128	1965.8	531.86	732.49	0.96593	1.9519	740.63	267.75
4	0.71924	2148.9	515.81	772.87	0.99991	2.5877	676.78	243.35
5	0.79732	14180	343.36	586.72	1.1283	3.4346	423.36	147.14
6	0.68175	3880.7	652.4	729.67	0.92523	2.746	937.54	237.4
7	0.68175	10494	627.95	722.25	0.92523	3.4325	916.94	223.46
8	0.6864	11865	594.48	718.16	0.93539	4.393	863.9	242.68
9	0.70652	4485.8	586.62	758.37	0.97612	5.6382	826.25	278.75
10	0.75048	39926	458.55	669.94	1.0542	8.62	531.26	94.324
11	0.66373	22489	621.51	673	0.88144	6.6271	889.7	119.33
12	0.66755	28550	657.35	721.59	0.8915	7.9198	923.61	120.97
13	0.67727	31675	632.46	700.63	0.91509	9.5442	935.56	190.99
14	0.69285	32392	619.16	706.09	0.94895	12.495	923.98	252.78
15	0.73844	84993	502.78	631.21	1.0339	18.429	580.48	74.382

rate sensitivity.

The methodology also predicts the process variables in the primary and secondary deformation zones. The predicted average strain, strain-rate, shear flow stress, and temperature both on the shear plane AB (primary deformation zone) and at the tool-chip interface (secondary deformation zone) are given with respect to the cutting test conditions in Table 10.

The methodology developed here is used in conjunction with orthogonal cutting tests that are obtained from the literature for Ti6Al4V titanium alloy and the detailed interfacial parameters are computed as shown in Table 11.

7 Conclusions

This paper utilizes an extended metal cutting analysis originally developed by Oxley and co-workers [6] and presents an improved methodology to expand applicability of the Johnson-Cook material model to the cutting regimes and simultaneously determine friction characteristics at the tool-chip interface from the results of orthogonal cutting tests.

A number of cutting temperature models are also used in characterizing the accuracy of the average temperatures at primary and secondary deformation zones. Predictions using various temperature models are compared with the results of orthogonal cutting test data obtained for AISI 1045 through assessment of machining models (AMM) activity [29]. The temperature model introduced by Oxley [6] is found most closely predicting the average temperature in shear plane and at the tool-chip interface.

The methodology developed for determining work flow stress and friction at tool-chip interface requires experimental data for cutting and thrust forces and chip thickness. The methodology is practical and computes both the parameters of work material Johnson-Cook constitutive flow stress model and the interfacial friction characteristics over the rake face. The extended Johnson-Cook work flow stress constants and tool-chip interfacial friction characteristics can be directly entered into most FEM software. This methodology has been effectively applied to characterize flow stress for AISI 1045 steel, Al6082-T6, and Ti6Al4V alloys at machining regimes and the friction parameters at the tool-chip interface by using the orthogonal cutting tests. The predicted flow stress at extended ranges is used in determining the constants of the Johnson-Cook constitutive material model. Therefore, the applicability of the Johnson-Cook material model for work material is extended beyond the typical ranges of SHPB tests.

Acknowledgment

The authors greatly acknowledge the financial support from NASA-New Jersey Space Grant Consortium under Grant No. NJSGC#02-41 to carry out this work.

Nomenclature

A = plastic equivalent strain in Johnson-Cook constitutive model (MPa)

a = power exponent of the normal stress distribution on the tool rake face

B = strain related constant in Johnson-Cook constitutive model (MPa)

Table 11 Computed parameters of C_0, δ and tool-chip interfacial friction (Ti6Al4V)

Test	C_0	δ	$\delta_{N\max}$ (N/mm^2)	l_p (mm)	l_c (mm)	a	μ_e
1	1.9591	0.0052	1726.2	0.1224	0.775	0.2218	0.4251
2	3.19	0.003	1558.3	0.0979	0.718	0.2187	0.4542
3	1.3872	0.0038	1850.5	0.0788	0.457	0.2203	0.4507
4	1.0756	0.0028	1996.1	0.0578	0.312	0.202	0.4227
5	4.147	0.0009	1178.2	0.0401	0.245	0.1747	0.4603
6	2.0586	0.0048	1754.8	0.1162	0.766	0.2202	0.398
7	4.3337	0.0018	1437.4	0.0929	0.912	0.1865	0.4482
8	3.7612	0.0018	1503.8	0.0719	0.593	0.2079	0.4546
9	2.9079	0.0028	1982.3	0.0541	0.299	0.2165	0.4547
10	5.1892	0.0005	1220.6	0.0334	0.297	0.134	0.3045
11	5.2629	0.0008	1227.8	0.1008	2.164	0.0946	0.3858
12	5.4666	0.0006	1289.1	0.0834	2.068	0.0818	0.4061
13	4.7957	0.001	1336	0.0675	0.812	0.1578	0.4387
14	3.5289	0.0014	1507.9	0.05	0.382	0.2155	0.4726
15	5.3357	0.0004	1134.3	0.0317	0.314	0.1227	0.2673

C = strain-rate sensitivity constant in the Johnson-Cook constitutive model
C_0 = strain rate constant proposed by Oxley
F_C, F_T = cutting and thrust force components (N)
F_F, F_N = frictional and normal force components at tool rake face (N)
F_S, F_{NS} = shear force and normal to the shear force components at AB (N)
K = work material thermal conductivity (W/m°C)
k_{AB} = shear flow stress on AB (N/mm^2)
k_{chip} = shear flow stress in the chip at the tool-chip interface (N/mm^2)
l_{AB} = length of the primary shear zone (mm)
l_c = length of the tool-chip contact (mm)
l_p = length of the sticking region (mm)
m = thermal softening parameter in the Johnson-Cook constitutive model
n = strain-hardening parameter in the Johnson-Cook constitutive model
p_A, p_B, p_M, p_N = hydrostatic stresses at the points A, B, M, and N (N/mm^2)
R_T = nondimensional thermal number
S = specific heat of work material (J/kg°C)
T_0 = initial work material temperature (°C)
T_{AB} = average temperature along AB (°C)
T_{int} = average temperature along the tool-chip interface (°C)
T_m = melting temperature of the work material (°C)
t_u, t_c = undeformed and deformed chip thickness (mm)
V, V_S, V_C = cutting velocity, shear velocity, and chip velocity (m/s)
w = width of cut (mm)
α = tool rake angle (deg)
β = proportion of the heat conducted into work material
δ = proportion of the thickness of the secondary zone to the chip thickness
$\bar{\varepsilon}_{AB}, \bar{\varepsilon}_{\text{int}}$ = effective strain at AB and tool-chip interface (mm/mm)
$\dot{\bar{\varepsilon}}_0$ = reference strain rate (s^{-1})
$\dot{\bar{\varepsilon}}_{AB}, \dot{\bar{\varepsilon}}_{\text{int}}$ = effective strain rate at AB and tool-chip interface (s^{-1})
ϕ = shear angle (deg)
$\bar{\gamma}_{AB}, \bar{\gamma}_{\text{int}}$ = effective shear strain at AB and tool-chip interface (mm/mm)
$\dot{\bar{\gamma}}_{AB}, \dot{\bar{\gamma}}_{\text{int}}$ = effective shear strain-rate at AB and tool-chip interface (s^{-1})
μ_e = coefficient of friction in the elastic contact region of tool-chip interface
ρ = density (kg/m^3)
σ_0 = initial yield strength of the material at room temperature (N/mm^2)
$\bar{\sigma}_{AB}$ = effective flow stress at AB (N/mm^2)
σ_N = normal stresses acting on the tool-chip interface (N/mm^2)
τ_{int} = frictional shear stress at the tool-chip interface (N/mm^2)
ψ = tool-chip interface temperature factor

Appendix: Slip-Line Field Analysis

The slip-line field analysis reveals the equilibrium equations as Eq. (A1) on the AB with a I slip-line and as Eq. (A2) on the MN with a II slip-line,

$$\frac{\partial p}{\partial s_1} + 2k\frac{\partial \psi}{\partial s_1} - \frac{\partial k}{\partial s_2} = 0 \tag{A1}$$

$$\frac{\partial p}{\partial s_2} - 2k\frac{\partial \psi}{\partial s_2} - \frac{\partial k}{\partial s_1} = 0 \tag{A2}$$

In the above equations p and k are the hydrostatic stress and shear flow stress of the work material, ψ is the angular rotation, and s_1 and s_2 are distances measured along I and II lines, respectively. Both lines AB and MN are assumed straight along slip-lines I and II, respectively. On line AB the equilibrium equation becomes Eq. (A3),

$$\frac{p_A - p_B}{l_{AB}} = \frac{dk}{ds_2} \tag{A3}$$

The right-hand side of Eq. (A3) can be written as Eq. (A4),

$$\frac{dk}{ds_2} = \frac{dk}{d\gamma}\frac{d\gamma}{dt}\frac{dt}{ds_2} \tag{A4}$$

Recall that shear flow stress is a function of strain, strain-rate, and temperature constituted by the Johnson-Cook model,

$$\frac{dk}{d\gamma} = k_{AB}\left[\frac{Bn}{\gamma_{AB}}\left(\frac{\gamma_{AB}}{\sqrt{3}}\right)^n\right] \Bigg/ \left[A + B\left(\frac{\gamma_{AB}}{\sqrt{3}}\right)^n\right] \tag{A5}$$

$$\frac{d\gamma}{dt} = \frac{C_0}{l_{AB}}\frac{V\cos\alpha}{\cos(\phi - \alpha)} \tag{A6}$$

$$\frac{dt}{ds_2} = \frac{1}{V\sin\phi} \tag{A7}$$

Substituting Eqs. (A4)–(A7) into Eq. (A3) yields Eq. (A8),

$$p_A - p_B = 2k_{AB}\frac{BnC_0}{A\varepsilon_{AB}^{-n} + B} \tag{A8}$$

Similarly, the equilibrium equation along line MN that is given with Eq. (A2) becomes Eq. (A9) when it is assumed to be straight, the strain-rate and temperature are considered unchanged in the secondary zone,

$$\frac{p_M - p_N}{l_{MN}} - 2\frac{k_{\text{chip}}(\phi - \alpha)}{l_{MN}} = \frac{dk}{ds_1} \tag{A9}$$

$$\frac{dk}{ds_1} = \frac{dk}{d\gamma}\frac{d\gamma}{dt}\frac{dt}{ds_1} \tag{A10}$$

$$\frac{dk}{d\gamma} = k_{\text{chip}}\left[\frac{Bn}{\gamma_{\text{int}}}\left(\frac{\gamma_{\text{int}}}{\sqrt{3}}\right)^n\right] \Bigg/ \left[A + B\left(\frac{\gamma_{\text{int}}}{\sqrt{3}}\right)^n\right] \tag{A11}$$

$$\frac{d\gamma}{dt} = \frac{V\sin\phi}{\delta t_c\cos(\phi - \alpha)} \tag{A12}$$

$$\frac{dt}{ds_1} = \frac{1}{V\sin(\phi - \alpha)} \tag{A13}$$

Substituting Eqs. (A10)–(A13) into Eq. (A9) yields Eq. (A14),

$$p_M - p_N = k_{\text{chip}}\left[2(\phi - \alpha) + \left(\frac{(Bn\varepsilon_{\text{int}}^n)/\gamma_{\text{int}}}{A + B\varepsilon_{\text{int}}^n}\right)\frac{l_p\sin\phi}{\delta t_c\sin(\phi - \alpha)}\right] \tag{A14}$$

References

[1] Ernst, H., and Merchant, M. E., 1941, "Chip Formation, Friction and High Quality Machined Surfaces," Trans. Am. Soc. Met., **29**, pp. 299–378.
[2] Lee, E. H., and Shaffer, B. W., 1951, "The Theory of Plasticity Applied to a Problem of Machining," J. Appl. Mech., **18**, pp. 405–413.
[3] Zorev, N. N., 1963, "Inter-Relationship Between Shear Processes Occurring Along Tool Face and Shear Plane in Metal Cutting," *International Research in Production Engineering*, ASME, New York, pp. 42–49.
[4] Tay, A. O., Stevenson, M. G., and de Vahl Davis, M. G., 1974, "Using the Finite Element Method to Determine Temperature Distributions in Orthogonal Machining," *Proceedings of the Institution for Mechanical Engineers*, **188**, pp.

627–638.
[5] Usui, E., and Shirakashi, T., 1982, "Mechanics of Machining: From Descriptive to Predictive Theory," *On the Art of Cutting Metals-75 Years Later*, ASME, New York, **PED 7**, pp. 13–35.
[6] Oxley, P. L. B., 1989, *Mechanics of Machining, an Analytical Approach to Assessing Machinability*, Ellis Horwood Limited.
[7] Özel, T., and Altan, T., 2000, "Determination of Workpiece Flow Stress and Friction at the Chip-Tool Contact for High-Speed Cutting," Int. J. Mach. Tools Manuf., **40/1**, pp. 133–152.
[8] Childs, T. H. C., 1998, "Material Property Needs in Modeling Metal Machining," in Proceedings of the CIRP International Workshop on Modeling of Machining Operations, Atlanta, Georgia, May 19, pp. 193–202.
[9] Jaspers, S. P. F. C., and Dautzenberg, J. H., 2002, "Material Behavior in Conditions Similar to Metal Cutting: Flow Stress in the Primary Shear Zone," J. Mater. Process. Technol., **122**, pp. 322–330.
[10] Adibi-Sedeh, A. H., Madhavan, V., and Bahr, B., 2003, "Extension of Oxley's Analysis of Machining to Use Different Material Models," ASME J. Manuf. Sci. Eng., **125**, pp. 656–666.
[11] Davies, M. A., Cao, Q., Cooke, A. L., and Ivester, R., 2003, "On the Measurement and Prediction of Temperature Fields in Machining 1045 Steel," CIRP Ann., **52**(1), pp. 77–80.
[12] Özel, T., and Altan, T., 2000, "Process Simulation Using the Finite Element Method: Prediction of Cutting Forces, Tool Stresses and Temperatures in High-Speed Flat End Milling Process," Int. J. Mach. Tools Manuf., **40/5**, pp. 713–738.
[13] Johnson, G. R., and Cook, W. H., 1983, "A Constitutive Model and Data for Metals Subjected to Large Strains, High Strain Rates and High Temperatures," *Proceedings of the 7th International Symposium on Ballistics*, The Hague, The Netherlands, pp. 541–547.
[14] Zerilli, F. J., and Armstrong, R. W., 1987, "Dislocation-Mechanics-Based Constitutive Relations for Material Dynamics Calculations," J. Appl. Phys., **61**(5), pp. 1816–1825.
[15] Hamann, J. C., Grolleau, V., and Le Maitre, F., 1996, "Machinability Improvement of Steels at High Cutting Speeds—Study of Tool/Work Material Interaction," CIRP Ann., **45**, pp. 87–92.
[16] Lee, W. S., and Lin, C. F., 1998, "High-Temperature Deformation Behavior of Ti6AL4V Alloy Evaluated by High Strain-Rate Compression Tests," J. Mater. Process. Technol., **75**, pp. 127–136.
[17] Meyer Jr, H. W., and Kleponis, D. S., 2001, "Modeling the High Strain Rate Behavior of Titanium Undergoing Ballistic Impact and Penetration," Int. J. Impact Eng., **26**, pp. 509–521.
[18] Shatla, M., Kerk, C., and Altan, T., 2001, "Process Modeling in Machining. Part I: Determination of Flow Stress Data," Int. J. Mach. Tools Manuf., **41**, pp. 1511–1534.
[19] Tounsi, N., Vincenti, J., Otho, A., and Elbestawi, M. A., 2002, "From the Basic Mechanics of Orthogonal Metal Cutting Toward the Identification of the Constitutive Equation," Int. J. Mach. Tools Manuf., **42**, pp. 1373–1383.
[20] Adibi-Sedeh, A. H., and Madhavan, V., 2002, "Effect of Some Modifications to Oxley's Machining Theory and the Applicability of Different Material Models," Mach. Sci. Technol., **6**(3), pp. 379–395.
[21] Lee, L. C., Liu, X., and Lam, K. Y., 1995, "Determination of Rake Stress Distribution in Orthogonal Machining," Int. J. Mach. Tools Manuf., **35**(3), pp. 373–382.
[22] Huang, Y., and Liang, S. Y., 2003, "Cutting Forces Modeling Considering the Effect of Tool Thermal Property-Application to CBN Hard Turning," Int. J. Mach. Tools Manuf., **43**, pp. 307–315.
[23] Trigger, K. J., and Chao, B. T., 1951, "An Analytical Evaluation of Metal Cutting Temperatures," Trans. ASME, **73**, pp. 57–68.
[24] Chao, B. T., and Trigger, K. J., 1953, "The Significance of the Thermal Number in Metal Machining," Trans. ASME, **75**, pp. 109–120.
[25] Leowen, E. G., and Shaw, M. C., 1954, "On the Analysis of Cutting Tool Temperatures," Trans. ASME, **71**, pp. 217–231.
[26] Leone, W. C., 1954, "Distribution of Shear Zone Heat in Metal Cutting," Trans. ASME, **76**, pp. 121–125.
[27] Boothroyd, G., 1963, "Temperatures in Orthogonal Metal Cutting," Proc. Inst. Mech. Eng., **177**, pp. 789–802.
[28] Komanduri, R., and Hou, Z. B., 2000, "Thermal Modeling of the Metal Cutting Process, Part I: Temperature Rise Distribution Due to Shear Plane Heat Source," Int. J. Mech. Sci., **42**, pp. 1715–1752.
[29] Ivester, R. W., Kennedy, M., Davies, M., Stevenson, R., Thiele, J., Furness, R., and Athavale, S., 2000, "Assessment of Machining Models: Progress Report," Mach. Sci. Technol., **4**(3), pp. 511–538.
[30] Bates, D., and Watts, D., 1988, *Nonlinear Regression Analysis and its Applications*, Wiley, New York, pp. 271–272.
[31] Barry, J., Byrne, G., and Lennon, D., 2001, "Observations on Chip Formation and Acoustic Emission in Machining Ti-6Al-4V Alloy," Int. J. Mach. Tools Manuf., **41**, 1055–1070.